Journal of Power Sources 232 (2013) 286–296

Contents lists available at SciVerse ScienceDirect

Journal of Power Sources

journal homepage: www.elsevier.com/locate/jpowsour

Promotional effect of Partial substitution of Zn by Ce in CuZnAlO catalysts used for hydrogen production via steam reforming of dimethyl ether

Lijie Zhang [a], Ming Meng [a,*], Shuang Zhou [a], Zhaosong Sun [a], Jing Zhang [b], Yaning Xie [b], Tiandou Hu [b]

[a] Tianjin Key Laboratory of Applied Catalysis Science and Engineering, School of Chemical Engineering and Technology, Tianjin University, Tianjin 300072, PR China
[b] Beijing Synchrotron Radiation Facility, Institute of High Energy Physics, Chinese Academy of Sciences, Beijing 100049, PR China

HIGHLIGHTS

- Substitution of Zn by Ce can improve the DME SR performance of CuZnAlO catalyst.
- The optimal content of CeO_2 in substituted CuZnAlCeO catalysts is 10% by weight.
- The presence of CeO_2 can enhance the dispersion and reducibility of Cu species.
- The catalyst with more Cu^+ species shows higher capability for CO chemisorption.

ARTICLE INFO

Article history:
Received 21 October 2012
Received in revised form
25 December 2012
Accepted 10 January 2013
Available online 21 January 2013

Keywords:
Dimethyl ether
Steam reforming
Hydrogen production
Copper-based catalyst
Substitution

ABSTRACT

A series of CuZnAlCeO catalysts with Zn partially substituted by Ce were prepared by co-precipitation, and employed for hydrogen production via dimethyl ether steam reforming (DME SR). The catalytic activity of these catalysts largely depends on CeO_2 content. The catalyst containing 10 wt% CeO_2 exhibits the best catalytic performance. The techniques of X-ray diffraction (XRD), N_2O chemisorption, X-ray absorption fine structure (XAFS, including XANES and EXAFS), temperature-programmed reduction (H_2-TPR) and CO desorption (CO-TPD) were used for catalyst characterization. The results of XRD, H_2-TPR and N_2O chemisorption conformably indicate that partial substitution of Zn by Ce can remarkably improve the dispersion of Cu species. The presence of Ce could not only inhibit the sintering of Cu species, but also improve the reducibility of copper oxides. The CO-TPD results clearly indicate that the two catalysts with 5 and 10 wt% CeO_2 possess higher CO-chemisorption capability than others, which is consistent with the results of Cu dispersion. The linear fitting results of XANES spectra reveal that these two catalysts also contain higher amount of Cu^+ species, which determines their better catalytic performance for DME SR.

1. Introduction

Nowadays, the increasing energy crisis and environmental pollution caused by fossil fuels combustion have greatly expedited the research and exploration of new energies and energy-clean-usage techniques. Among them, H_2-based fuel cells such as proton exchange membrane fuel cells (PEMFCs) are getting more and more attention in the area of electric vehicles due to their high energy density, rapid start up, compact size and zero pollution [1,2]. However, the supply of H_2 is still remaining a problem. It is known that H_2 is very hard to be compressed into liquid, the usage of ready-made H_2 means that the vehicles will go everywhere with very high pressure tanks, which greatly increases the cost and the danger induced by H_2 leak. So, it is highly expected that the H_2 can be produced onboard via some H_2-rich materials. Up to now, the most promising technique for hydrogen production onboard is catalytic reforming; and many kinds of H_2-containing materials including methane, liquefied petroleum gas (LPG), gasoline, ethanol (EtOH), methanol (MeOH) and dimethyl ether (DME) have been employed to produce hydrogen through catalytic reforming technique. Among these materials, DME is the most attractive one which possesses many intrinsic merits such as high H/C ratio, high energy density, no toxicity, no carcinogenicity, and less coke formation due to the lack of C–C bond in its molecule [3,4]. In

* Corresponding author. Tel./fax: +86 (0)22 2789 2275.
E-mail address: mengm@tju.edu.cn (M. Meng).

0378-7753/$ – see front matter © 2013 Elsevier B.V. All rights reserved.
http://dx.doi.org/10.1016/j.jpowsour.2013.01.071

addition, DME can be reformed at much lower temperature (about 250–400 °C) than other hydrocarbons, which makes it more suitable for hydrogen production onboard. Although MeOH can also be reformed at low temperature, it possesses toxicity and shows much lower mass or volume specific energy density than DME. Moreover, the well-developed infrastructure for LPG can be readily adapted for DME due to the similarity of their physical properties. Therefore, DME is now regarded as the most promising raw material for hydrogen production onboard.

It is known that the reforming of hydrocarbons can be operated at different modes including steam reforming (SR), partial oxidation (POX) and autothermal reforming (ATR). Among them, steam reforming does not require oxygen and produces reformates with more hydrogen than POX and ATR. Freni and co-workers first reported the production of hydrogen from DME SR [5]. They proved the possibility of production of hydrogen-rich mixtures by DME SR reaction. Park and co-workers ever combined DME SR system and lean NO_x trap, greatly improving NO_x reduction in DME engines [6].

The steam reforming of DME as shown in reaction (1) consists of two moderate endothermic reactions in sequence, namely DME hydrolysis to methanol (reaction (2)) and methanol steam reforming to hydrogen and carbon dioxide (reaction (3)). During DME steam reforming, some side reactions might occur [7,8], such as reverse water–gas shift reaction (r-WGS) as shown in reaction (4).

DME steam reforming

$$(CH_3)_2O + 3H_2O \rightarrow 6H_2 + 2CO_2 \qquad \Delta H^{\ominus} = 135\ \text{kJ mol}^{-1} \tag{1}$$

DME hydrolysis

$$(CH_3)_2O + H_2O \rightarrow 2CH_3OH \qquad \Delta H^{\ominus} = 37\ \text{kJ mol}^{-1} \tag{2}$$

MeOH steam reforming

$$CH_3OH + H_2O \rightarrow 3H_2 + CO_2 \qquad \Delta H^{\ominus} = 49\ \text{kJ mol}^{-1} \tag{3}$$

Reverse water–gas shift reaction

$$CO_2 + H_2 \rightarrow CO + H_2O \qquad \Delta H^{\ominus} = 41\ \text{kJ mol}^{-1} \tag{4}$$

Thus, bifunctional catalysts consisting of a DME hydrolysis catalyst (solid acid such as alumina, zeolite and so on) and a MeOH steam reforming catalyst (Cu-, Pt-, or Pd-based catalysts) are generally required for DME steam reforming. Several kinds of strong solid acids such as zeolite and heteropoly acid have ever been employed as DME hydrolysis catalysts [9–11]. It is found that these strong solid acids could result in serious coke on catalyst surface, decreasing the catalytic activity and durability of the catalysts. In comparison, the acidity of γ-Al_2O_3 seems to be more appropriate for DME hydrolysis, which can effectively inhibit the formation of coke, as a result, the catalyst durability is remarkably improved [9,12]. For MeOH steam reforming, several kinds of metal catalysts have been extensively studied such as copper and noble metal (Pd, Rh and Pt) catalysts [13]. Although noble metal catalysts often show high activity, the disadvantages such as high cost and high selectivity to CO restrain their application. On the contrary, Cu-based catalysts, especially CuZn-based ones have been widely applied to various reactions such as MeOH synthesis [14], MeOH SR [15], MeOH oxidative steam reforming [16,17], water–gas shift reaction [18], and DME SR [19], due to their high catalytic activity and low cost. However, Cu-based catalysts often exhibit low thermal stability; at the temperature above 300 °C, they can gradually get agglomerated, leading to obvious decrease of Cu dispersion and catalytic activity. At present, it is still a big challenge to improve the thermal stability of Cu-based catalysts. Eguchi et al. [20] found that the copper species in complex oxide $CuFe_2O_4$ show not only high catalytic activity but also high stability during DME SR. Ma et al. [21] prepared a series of Cu–Ni/γ-Al_2O_3 catalysts by the deposition–precipitation method, and found that the presence of Ni could retard the sintering of copper and thus improve the durability of the catalysts. It is well known that CeO_2 is usually used in catalysts as promoter due to its excellent redox property, high oxygen storage capacity (OSC), strong interaction with other supported metals [22], so, it is often added to Cu-containing catalysts. As reported, ceria could increase the dispersion and reducibility of copper species, improving the activity and thermal stability of the catalysts; meanwhile, the addition of ceria could also reduce the CO concentration during the oxidative steam reforming of methanol [17]. For the preferential oxidation of CO in H_2-rich stream the combined copper–ceria catalysts are particularly active, showing not only excellent oxidation activity but also high selectivity of oxygen to CO_2 [23].

Therefore, in this work, ceria is selected as a promoter added to CuZnAlO oxide catalysts. It is expected that the incorporation of ceria in CuZnAlO catalysts can improve their catalytic performance for DME SR including DME conversion, hydrogen yield, CO_2 selectivity and catalyst durability. Based on the results of activity evaluation and catalyst characterization such as XRD, H_2-TPR, N_2O chemisorption, XAFS (EXAFS and XANES) and CO-TPD, the content of Ce in the catalysts is optimized and the effect of ceria substitution on the catalytic performance of the catalysts is investigated in detail.

2. Experimental

2.1. Catalyst preparation

A series of CuZnAlCeO mixed oxide catalysts were prepared by co-precipitation using Na_2CO_3 as precipitating reagent. The contents of CuO, Al_2O_3 and ZnO in the catalyst CuZnAlO were 30 wt%, 10 wt% and 60 wt%, respectively. In Ce-substituted catalysts CuZnAlCeO the contents of CuO and Al_2O_3 were kept unchanged but that of ZnO was decreased due to the partial substitution of ZnO by CeO_2. Several contents of CeO_2 such as 5, 10, 20, 30 and 40 wt% were adopted for optimization. According to above stoichiometry a mixed nitrate solution containing $Cu(NO_3)_2\cdot 3H_2O$, $Zn(NO_3)_2\cdot 6H_2O$, $Ce(NO_3)_3\cdot 6H_2O$ and $Al(NO_3)_3\cdot 9H_2O$ was first prepared at room temperature. Under vigorous stirring the aqueous solution of 0.5 M Na_2CO_3 was added dropwise to the mixed solution until the pH reached 7.0. Then the solution containing precipitate was aged at 70 °C for 2 h. After filtration, the obtained precipitate was washed with distilled water for three times, and dried at 120 °C for 12 h. At last, the dry precursor was calcined in air at 500 °C for 4 h to get the final catalyst CuZnAlCeO. For simplicity, the catalysts are denoted as $CuZnAlCe_x$ (x = 0, 0.05, 0.1, 0.2, 0.3 or 0.4), where x represents the weight content of CeO_2 in the catalysts. The $CuZnAlCe_x$ catalysts were mechanically mixed with γ-Al_2O_3 (supplied by Tianjin Chemical Research & Design Institute, S_{BET} = 189 $m^2\ g^{-1}$) at a fixed weight ratio of 2:1. Before use for activity measurement, this mixture was pressed, grounded and sieved to 40–60 mesh.

2.2. Catalyst activity–durability evaluation

The catalytic activity of the catalysts for DME SR was evaluated in a fixed-bed continuous flow reactor containing 500 mg sample.

All the catalysts were first pretreated at 300 °C for 1 h in 10% H_2/N_2 mixture gas prior to the activity evaluation. The feedstock for DME SR consists of 40% N_2, 50% H_2O (g) and 10% DME ($S/C = 2.5$) with a constant space velocity of 12,000 mL h^{-1} g_{cat}^{-1}. The external and internal mass transfer limitations have already been excluded by variation of the linear flow rate over the catalyst and the catalyst particle size, respectively. Compositions of influent and effluent gas were analyzed by an on-line gas chromatograph (GC) (Agilent 7890A) which was equipped with three detectors, one hydrogen flame ionization detector (FID) and two thermal conductivity detectors (TCD). Totally six columns were used for composition analysis: three ProPak N columns, two MolSieve 5A columns and a PoraPak Q capillary column. The Porapak Q capillary column was used to separate CH_4, DME and CH_3OH. A molSieve 5A column was used for H_2 analysis. The rest of columns were used to separate CO_2, CO and N_2. Before analysis, the effluents from reactor were purified by a trap filled with $Mg(ClO_4)_2$ to remove the H_2O. These catalysts after activity tests are defined as spent catalysts. The DME conversion and the selectivity to C1 species are defined as follows:

$$X_{DME} = \frac{F_{DME,in} - F_{DME,out}}{F_{DME,in}} \times 100\%$$

$$S_{Ci} = \frac{F_{Ci}}{\sum F_{Ci}} \times 100\%$$

$F_{DME,in}$ and $F_{DME,out}$ are the influent and effluent molar flow rates of DME, respectively, and F_{Ci} is the effluent molar flow rate of C1-containing products, including CH_3OH, CH_4, CO, and CO_2.

Hydrogen yield is defined as a molar ratio of experimental production to theoretical production of hydrogen per molar DME feed.

$$Y_{H_2} = \frac{F_{H_2}}{F_{DME,in}} \times \frac{1}{6} \times 100\%$$

F_{H_2} is the effluent molar flow rate of H_2.

Long-term durability tests for the catalysts $CuZnAlCe_0$ and $CuZnAlCe_{0.1}$ were carried out to investigate the deactivation behavior in the following manner. The reaction temperature was kept at 400 °C. The composition of feed gas was the same as that for activity tests. These catalysts after durability tests were defined as degraded catalysts.

2.3. Catalyst characterization

The specific surface area and pore structure of the catalysts were measured by nitrogen physisorption at 77 K on a Quantachrome QuadraSorb SI instrument. Before measurement the samples were degassed under vacuum at 300 °C for 6 h. The specific surface area was calculated using standard BET method in 0–0.3 partial pressure range. The average pore diameter and pore volume were calculated by using the Barrett–Joyner–Halenda (BJH) method based on desorption isotherm.

For the spent catalysts and pre-reduced samples, to avoid the potential oxidation of metallic copper at room temperature after exposure to air, the samples were cooled in highly pure N_2 atmosphere, kept in a container which was filled with highly pure N_2, and employed for other characterization measurements (BET, H_2-TPR and XAFS) as soon as possible.

X-ray diffraction measurement was carried out on a D8 diffractometer (Bruker Company) using Cu Kα ($\lambda = 0.15418$ nm) as radiation source. The operating voltage and current are 40 kV and 40 mA, respectively. The diffraction data of 2θ from 20° to 90° were collected with a step size of 0.02°.

Temperature-programmed reduction by H_2 (H_2-TPR) and temperature-programmed desorption of CO (CO-TPD) were performed on the catalysts by using a XianQuan TP-5079 instrument equipped with a thermal conductivity detector. For H_2-TPR experiments, each time the quartz tube reactor was loaded with 30 mg powder sample (40–60 mesh) and heated from room temperature to 500 °C in the atmosphere of 8% H_2/N_2 (v/v) with a flow rate of 30 mL min^{-1}. Before detected by TCD, the water was eliminated by a trap containing CaO + NaOH. For CO-TPD experiments, 50 mg catalyst was first pre-reduced with 8% H_2/N_2 (v/v) at 300 °C for 30 min; then flushed for 1 h in highly pure He (99.99%, 50 mL min^{-1}) to remove physisorbed substances. After the catalyst bed returned to ambient temperature, 5% CO/He (50 mL min^{-1}) was injected to the sample cell for CO adsorption. The catalyst was flushed again for 1 h in He (50 mL min^{-1}) to remove the physisorbed CO. As the baseline was stable the temperature-programmed desorption of CO was carried out from room temperature to 700 °C at a heating rate of 10 °C min^{-1}.

Copper metal surface areas in the samples were determined by the N_2O decomposition method at 90 °C as reported by Jensen et al. [24], assuming a reaction stoichiometry of two Cu atoms per O atom and a Cu surface density of 1.46×10^{19} atom m^{-2} [25]. Each sample after reduced at 300 °C in an 8% H_2/N_2 mixture and then flushed with He (50 mL min^{-1}) for 30 min, was first treated with 50% N_2O/N_2 mixture at 90 °C for 1 h, then TPR was carried out in an 8% H_2/N_2 mixture at rate of 10 °C min^{-1}. The amount of chemisorbed O atoms was determined from the area of the TPR peak.

X-ray absorption near-edge structure (XANES) and extended X-ray absorption fine structure (EXAFS) measurements were carried out on the XAFS station in the 1W1B beamline of Beijing Synchrotron Radiation Facility (BSRF) operating at about 150 mA and 2.2 GeV. The absorption spectra of the Cu K-edge of the samples and reference compounds were recorded at room temperature in transition mode. During the experiments, a copper foil was employed for energy calibration. A Si (111) double-crystal monochromator was used to reduce the harmonic content of the monochrome beam. The back-subtracted EXAFS function was converted into k space and weighted by k^3 in order to compensate for the diminishing amplitude due to the decay of the photoelectron wave. The Fourier transforming of the k^3-weighted EXAFS data was performed in the range of $k = 3$–13 $Å^{-1}$ using a Hanning window function. A linear combination fitting (LCF) was performed on the XANES spectra using the corresponding spectra of metallic Cu (Cu foil), Cu_2O and CuO as standards. All the data are analyzed by the software Arthana.

3. Results and discussion

3.1. Catalyst characterization

3.1.1. Texture data and copper dispersion

The specific surface area and pore volume of various catalysts, as well as the surface area and dispersion of metallic copper are shown together in Table 1. No significant difference in the BET surface area is observed among all the catalysts. However, obvious difference in the surface area and dispersion of metallic copper is clearly observed. The catalyst containing 10 wt% CeO_2 exhibits the highest surface area and highest dispersion of metallic copper. After addition of 10% CeO_2 to CuZnAlO the surface area of Cu^0 is remarkably increased from 20.6 to 57.4 m^2 g^{-1}. Similar result was also obtained in CeO_2-promoted CuO/Al_2O_3 catalysts by Fernández-García et al. [26]. However, addition of excessive Ce ($CeO_2 \geq 20$ wt %) results in gradual decrease of Cu surface area and dispersion.

Table 1
Specific surface area (SSA), pore volume (PV), Cu surface area (S_{Cu}), Cu dispersion (D_{Cu}), Cu crystallite size in spent catalysts ($t_{Cu,s}$) and degraded catalysts ($t_{Cu,d}$), relative amounts of desorbed CO (ADC) during CO-TPD, and apparent activation energy of $CuZnAlCe_x$ catalysts.

Sample	SSA ($m^2\ g^{-1}$)	PV ($cc\ g^{-1}$)	S_{Cu} ($m^2\ g^{-1}$)[a]	D_{Cu} (%)[a]	$t_{Cu,s}$ (nm)[b]	$t_{Cu,d}$ (nm)[c]	ADC[d]	E_a ($kJ\ mol^{-1}$)[e]
$CuZnAlCe_0$	90.1	0.20	20.6	13.3	15.5	20.3	1.00	136.3
$CuZnAlCe_{0.05}$	93.0	0.24	45.4	20.3	8.0	–	1.87	142.2
$CuZnAlCe_{0.1}$	95.3	0.29	57.4	24.0	9.2	13.3	2.15	147.9
$CuZnAlCe_{0.2}$	97.7	0.21	52.2	21.7	14.1	–	1.63	129.2
$CuZnAlCe_{0.3}$	93.1	0.22	38.8	17.2	13.7	–	1.61	127.2
$CuZnAlCe_{0.4}$	98.2	0.19	28.1	11.8	14.5	–	0.65	123.9

[a] Cu surface area (S_{Cu}) and Cu dispersion (D_{Cu}) were determined by TPR-N_2O titration method.
[b] Cu particle sizes ($t_{Cu,s}$) of spent catalysts were calculated from the value of full width at half maximum (FWHM) of the diffraction peaks for Cu (111) planes.
[c] Cu particle sizes ($t_{Cu,d}$) of degraded catalysts were calculated from the value of full width at half maximum (FWHM) of the diffraction peaks for Cu (111) planes.
[d] CO desorption amount was evaluated from the area of the peaks centered around 363 °C in the CO-TPD profiles.
[e] Apparent activation energy (E_a) was estimated from Arrhenius equation based on the activity.

This is probably due to the agglomeration of CeO_2 itself, as shown in the XRD patterns in the next section.

3.1.2. XRD characterization

To establish a correlation between the catalytic properties and active phases, XRD technique was employed to examine the bulk structure of the fresh catalysts, spent catalysts and degraded catalysts, respectively. As shown in Fig. 1(a), all the fresh catalysts exhibit typical diffraction patterns of ZnO and CuO, the ones with more than 5 wt% CeO_2 also exhibit the diffraction peaks of CeO_2 fluorite phase. By comparing the diffraction patterns of different catalysts, it can be found that with the increase of Ce content the diffraction peaks for ZnO phase gradually decrease, mainly due to the continuous reduction of ZnO content in the catalysts. In addition, the peaks of CuO remarkably decrease with the addition of CeO_2 to the catalysts, especially for the catalyst containing 10 wt% CeO_2. However, excessive amount of CeO_2 (≥20 wt%) results in the evolution of the diffraction

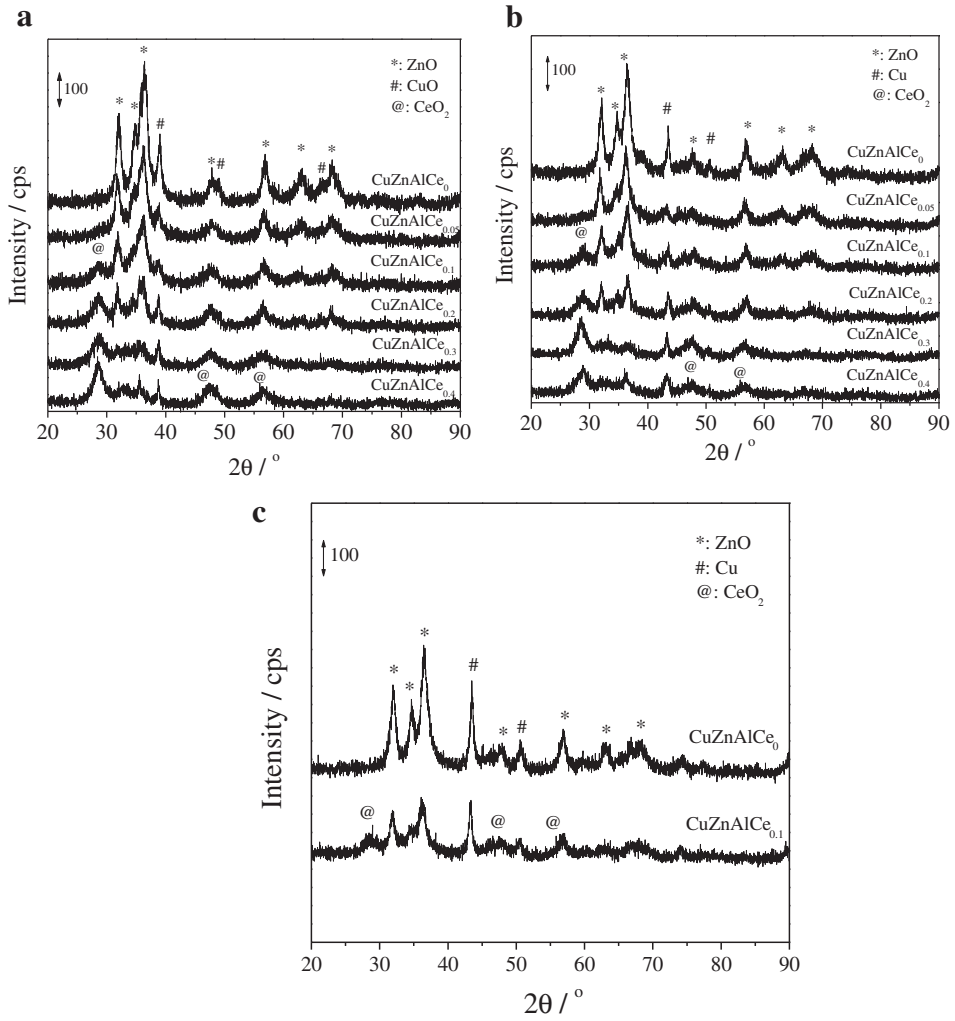

Fig. 1. XRD patterns of the $CuZnAlCe_x$ catalysts in different states: (a) fresh; (b) spent; (c) degraded after 48 h durability test.

peaks for CuO and CeO_2 phases, indicating the growth of CuO and CeO_2 crystallites.

The XRD patterns of the spent catalysts are shown in Fig. 1(b). Only diffraction peaks corresponding to metallic Cu, ZnO and CeO_2 are identified, indicating that metallic copper may be the main active phase of the present $CuZnAlCe_x$ catalysts for DME SR reaction. It should be noted that although no peaks of Cu_2O are detected, its existence cannot be excluded because it may exist in amorphous state. The Cu crystallite sizes estimated from the XRD patterns of spent catalysts by using Scherrer equation (see Table 1) indicate that Ce addition reduces the crystallite size of metallic Cu. The appropriate amount of CeO_2 in the catalysts should be 5 or 10 wt%. Further increase of CeO_2 content leads to the growth of metallic copper crystallites. The smaller the Cu crystallite size is, the higher the copper dispersion is.

Since the catalyst $CuZnAlCe_{0.1}$ exhibits the highest activity for DME SR, it was selected for a durability test for 48 h (see Section 3.1 for details). After durability test this sample was also characterized by XRD, the result of which is shown in Fig. 1(c). For comparison, the XRD pattern of the degraded catalyst $CuZnAlCe_0$ is also included in this figure. From Fig. 1(c), it is found that the diffraction peaks of metallic Cu for the degraded catalysts are much sharper and higher as compared with those of the spent catalysts, which suggests the serious sintering of metallic Cu. From the data listed in Table 1, it can still be seen that the size of Cu crystallites in $CuZnAlCe_0$ catalyst obviously increases from 15.5 to 20.3 nm after durability test, while for $CuZnAlCe_{0.1}$ catalyst it only grows from 9.2 to 13.3 nm. The existence of CeO_2 has greatly improved the stability of metallic copper phase during long-term durability test. Fernández-García et al. ever obtained similar result on CeO_2-promoted alumina-supported copper catalysts [26].

3.1.3. Cu K-edge XANES and EXAFS

To further confirm the fine structures of copper species, the XAFS technique including XANES and EXAFS was employed to characterize the catalysts as well as the reference materials (Cu foil, Cu_2O and CuO). The Cu K-edge XANES spectra of fresh catalysts are shown in Fig. 2(a). It is obvious that the XANES spectra of the catalysts are similar to that of CuO. However, the Cu K-edge XANES spectra of the spent catalysts as seen in Fig. 2(b) are more similar to that of metallic Cu with the main absorption peaks (1s → 4p) appearing at about 8995 and 9003 eV. In addition, there is also a pre-edge absorption peak appearing at ~8982 eV, which is assigned to a dipole-forbidden 1s → 3d transition [27]. These results suggest that the copper species in spent catalysts mainly exist

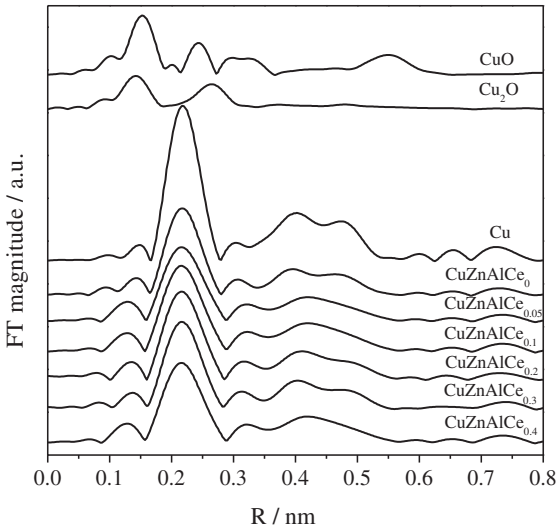

Fig. 3. Radial structure functions (RSFs) derived from Cu K-edge EXAFS spectra of the spent $CuZnAlCe_x$ catalysts and reference compounds.

in metallic state, which is totally consistent with the XRD results. The radial structure functions (RSFs) of Cu K-edge derived from EXAFS spectra of spent catalysts are shown in Fig. 3. It is found that the Cu K-edge RSFs of the spent catalysts are also analogous to that of metallic Cu, further confirming the copper species mainly existing in metallic state. The strongest coordination peaks at ~0.22 nm (without phase-scattering shift correction) could be assigned to the first Cu–Cu coordination shell in Cu^0. The coordination peaks between 0.10 and 0.15 nm in the RSFs are possibly contributed by the Cu–O shell in Cu_2O and/or CuO, however, they are so weak that it is hard to confirm whether there are small amounts of Cu_2O and/or CuO in the spent catalysts. Therefore, a LCF was performed on the XANES spectra of the spent catalysts using the corresponding spectra of metallic Cu, Cu_2O, and CuO as standards. Fernández-García et al. [28] and Bazin et al. [29] reported that the XANES shapes for Cu clusters with less than ca. 50 atoms are quite different from the metallic Cu (Cu foil). For clusters containing more atoms, such size effects become negligible. It means that the LCF results may be biased by such size-related effects when dealing with crystallites small enough. Since the catalysts employed in this work have relatively high copper loading and relatively large metallic copper crystallites formed from the pre-

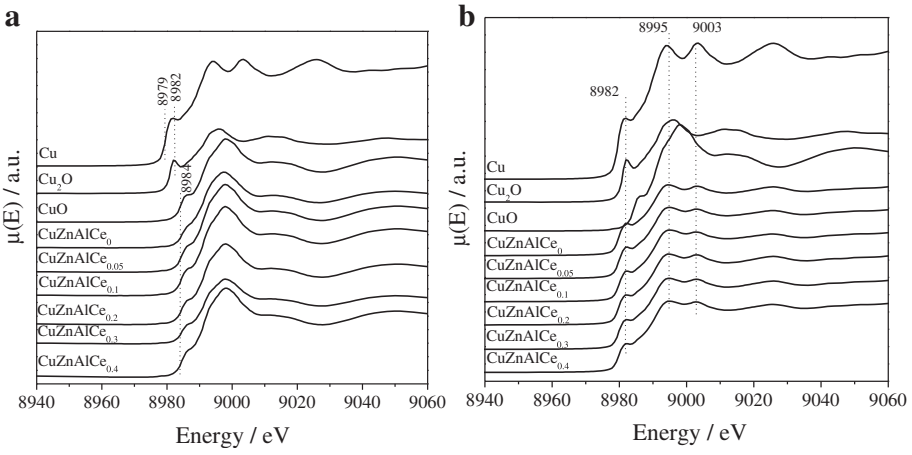

Fig. 2. Cu K-edge XANES spectra of the $CuZnAlCe_x$ catalysts in different states: (a) fresh; (b) spent.

reduction procedure [30], the LCF method could be used for the analysis of XANES spectra. The fitting results are shown in Fig. 4 and summarized in Table 2. It can be seen that after used in DME SR reaction Cu species mainly exist as Cu^0 with a small amount of Cu^+ and Cu^{2+} coexisting. These Cu^+ and Cu^{2+} species may be highly dispersed in the catalysts or exist in amorphous state so that the XRD measurements could not detect them. From Table 2, it is also found that the amounts of Cu^0 in the two catalysts $CuZnAlCe_{0.05}$ and $CuZnAlCe_{0.1}$ are obviously lower than those in other catalysts; however, the amounts of Cu_2O in these two catalysts are higher. In addition, it should be noted that the contents of CuO in all the substituted catalysts are increased after the addition of CeO_2 to them. The above results suggest that the addition of appropriate amount of CeO_2 in CuZnAl catalyst could adjust the valence and relative contents of copper species. As reported [31], different intermediates are often formed on different active sites, thus resulting in various products; the formation of CH_3O species mainly occurs on Cu^0 sites; while $HCOO^-$ and COO^- intermediates are

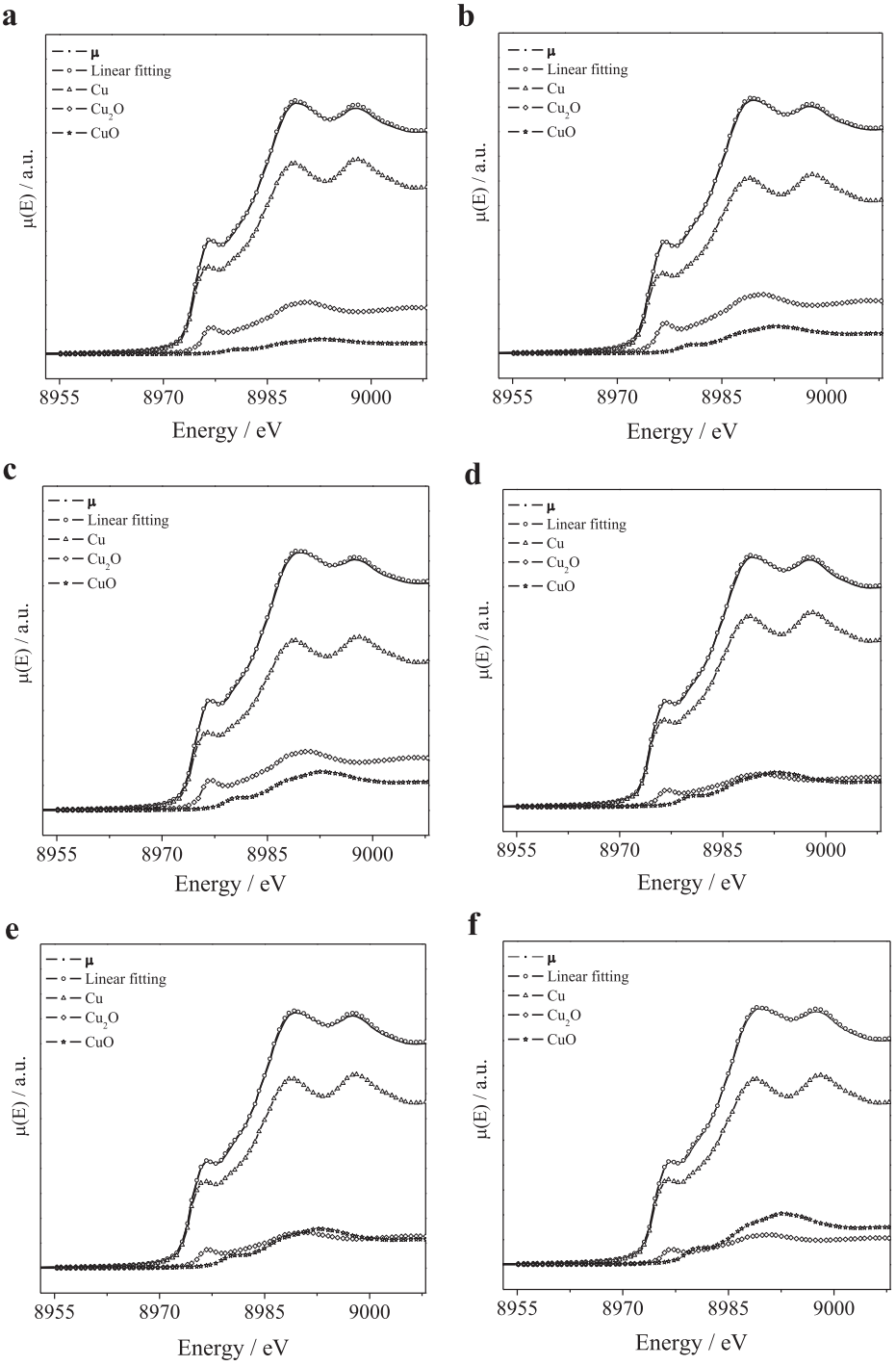

Fig. 4. XANES spectra (solid line) and fitting curves (dotted lines) for different catalysts after used in DME SR reaction: (a) $CuZnAlCe_0$; (b) $CuZnAlCe_{0.05}$; (c) $CuZnAlCe_{0.1}$; (d) $CuZnAlCe_{0.2}$; (e) $CuZnAlCe_{0.3}$; (f) $CuZnAlCe_{0.4}$.

Table 2
Relative contents of different Cu species in the spent $CuZnAlCe_x$ catalysts obtained by the linear combination fitting of XANES spectra.

Sample	Cu (%)	Cu_2O (%)	CuO (%)
$CuZnAlCe_0$	76.8	18.7	4.6
$CuZnAlCe_{0.05}$	70.4	21.2	8.4
$CuZnAlCe_{0.1}$	67.4	20.9	11.8
$CuZnAlCe_{0.2}$	77.2	12.0	10.8
$CuZnAlCe_{0.3}$	75.3	12.7	12.0
$CuZnAlCe_{0.4}$	73.8	10.6	15.6

mainly generated on Cu^+ sites. The decomposition of the intermediates $HCOO^-$ and COO^- can produce CO_2, leading to high CO_2 selectivity. In this work, the addition of CeO_2 to the catalysts $CuZnAlCe_{0.05}$ and $CuZnAlCe_{0.1}$ is favorable to the formation of Cu^+ species; so, it is inferred that the CO_2 selectivity should be partially contributed by Cu^+ species.

3.1.4. H_2-TPR results

The H_2-TPR profiles of the fresh catalysts are displayed in Fig. 5(a). According to the literature [32,33], the surface ceria could be reduced at significantly lower temperature in the presence of copper. To make clear that if the reduction of ceria has taken place during TPR, quantitative estimation on H_2 consumption was performed. The overall H_2 consumptions of 3641, 3867, 4025, 4184, 4294, and 4383 μmol g^{-1} catalyst for $CuZnAlCe_0$, $CuZnAlCe_{0.05}$, $CuZnAlCe_{0.1}$, $CuZnAlCe_{0.2}$, $CuZnAlCe_{0.3}$ and $CuZnAlCe_{0.4}$ were obtained, respectively. However, even though all Cu exists in the form of Cu^{2+}, the reduction of Cu only requires 3750 μmol g^{-1} for $CuZnAlCe_x$. In addition, it can be seen that the H_2 consumption increases with the elevation of Ce loading. So, it is deduced that the partial reduction of ceria should have occurred during TPR. The presence of copper could promote the reduction of ceria at lower temperature. As reported in the literature [32], the different peaks of copper–ceria must be related to structural or morphological differences. In this work, the multiple peaks observed can be attributed to the reduction of several kinds of copper oxides species in the samples. The reduction of reference compounds CuO and Cu_2O was also performed at the same condition, the results of which (not shown) indicate that pure CuO exhibits a single reduction peak at 370 °C while pure Cu_2O shows two reduction peaks appearing at 406 and 520 °C. In comparison, the copper species in $CuZnAlCe_0$ catalyst were reduced at much lower temperatures (250 and 263 °C). After addition of CeO_2 to the catalysts, the reduction temperature is further decreased; meanwhile, the two main reduction peaks gradually combine into one with the increase of CeO_2 content. Breen et al. ever reported that highly dispersed CuO species could be reduced at much lower temperature than bulk CuO [34]. Thus, the very broad and very weak reduction peaks between 204 and 220 °C are attributed to highly dispersed CuO species. By careful observation, it is still found that the area of the peaks for such CuO species increases and the reduction temperature decreases gradually with the elevation of CeO_2 content. Dow et al. [35] thought that there exists strong interaction between copper oxides and ceria at their interfaces (interfacial metal oxide–support interaction (IMOSI)), which can enhance not only the dispersion but also the reducibility of copper oxides. The second peaks around 235–240 °C are ascribed to the reduction of bulk-like CuO species, which weakly interact with the supports. It is well known that the interaction between Cu and Al oxides is rather strong, making the reduction of copper species relatively more difficult [36]. So, the third peaks between 250 and 258 °C are assigned to the reduction of copper oxides strongly interacted with alumina. It is interesting that with the increase of

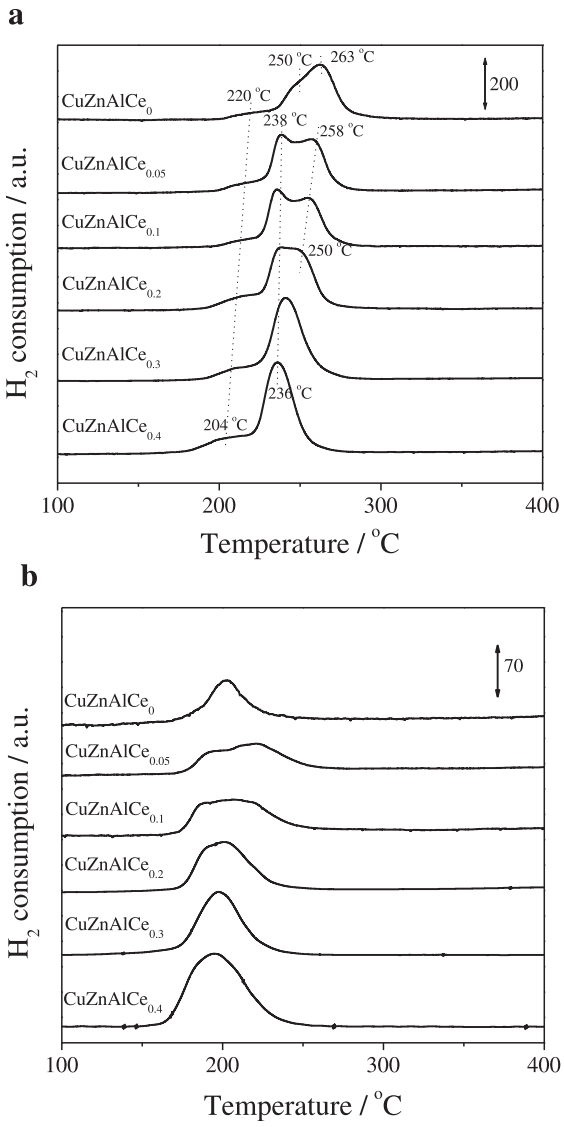

Fig. 5. H_2-TPR profiles of the $CuZnAlCe_x$ catalysts in different states: (a) fresh catalysts; (b) spent catalysts.

CeO_2 content in the catalysts the third peaks shift to lower temperatures until they totally overlap with the second ones, which suggests that more CeO_2 can weaken the interaction between copper oxides and alumina more obviously.

The spent catalysts show different reduction profiles from the fresh ones, as shown in Fig. 5(b). The appearance of reduction peaks means that there are still some reducible species such as Cu^+ or Cu^{2+} in the spent catalysts. It is worth noting that before used for DME SR all the catalysts were pre-reduced at 300 °C, which has caused full reduction of copper to metallic state according to TPR results shown in Fig. 5(a). It is reported that the chemical state of $Cu/ZnO/Al_2O_3$ catalysts is strongly affected by the reactant mixture [37]. The presence of Cu^+ or Cu^{2+} species is mainly resulted from the reoxidation of metallic copper by the water vapor at relatively high temperature as reported by other researchers [38]. It should be indicated that in the spent catalysts the Cu oxides may be also come from the oxidation of metallic copper by air after exposure to air for measurements. To make clear this point, the *ex situ* H_2-TPR measurements of the pre-reduced samples were carried out. There is no any obvious reduction signal detected in the H_2-TPR profiles,

indicating no significant oxidation after exposure to air at room temperature. So, it is deduced that in the spent catalysts the Cu oxides mainly come from the reoxidation of metallic copper by the water vapor during DME SR. Compared with those of the fresh catalysts, the H_2-TPR profiles of the spent ones have changed a lot such as the shape, area and position, which suggests obvious variation of the copper species during DME SR process. These results are totally consistent with those of EXAFS and XANES. The much lower area of the reduction peaks for spent catalysts indicates that most copper species still exist in metallic state during the reaction. The much lower reduction temperature (around 200 °C) shows that these Cu^+ or Cu^{2+} oxides possess much better reducibility. Similar phenomenon was also found on Co and Mn promoted Cu/CeO_2 systems during DME SR [38].

3.1.5. CO-TPD analysis

The CO-TPD profiles of the reduced catalysts are presented in Fig. 6. After reduction, the surface oxygen species could be removed, so, the formation of CO_2 after CO adsorption at room-temperature should be very little or neglectable. Additionally, the effluent gas from the TPD reactor was first purified by a CaO + NaOH trap, then entered the TCD for detection, so, the CO-TPD peaks should totally correspond to CO desorption. As reported in the literature [18,39], weakly chemisorbed CO is detected around 82 °C for all the catalysts. The desorption of chemisorbed CO mainly occurs between 200 and 500 °C with the peak zenith appearing around 360 °C. According to the work of Kam et al. [18], the CO-TPD spectra on the reduced Cu/ZnO catalysts exhibited a small peak at 60–80 °C and a dominant peak at 300–320 °C. Since CO did not chemisorb on ZnO in the Cu-containing catalysts [18], the peaks centered at 82 and 363 °C are naturally attributed to the desorption of CO chemisorbed on copper sites. For the Ce-containing catalysts in this work, a small peak at about 146 °C was also observed. It is reported [40] that linear CO can adsorb on Ce^{3+} ions generated after reduction. So, the desorption peak centered at 146 °C may correspond to the desorption of CO adsorbed on cerium ions. Concerning the desorption peaks centered at 363 °C, except for the catalyst $CuZnAlCe_{0.4}$, other Ce-containing catalysts show larger desorption peak than $CuZnAlCe_0$ (as listed in Table 1), especially for the two catalysts $CuZnAlCe_{0.05}$ and $CuZnAlCe_{0.1}$. This result is in good accordance with that of Cu dispersion for these catalysts.

3.2. Catalytic performance

3.2.1. Steam reforming of dimethyl ether (DME SR)

Fig. 7 demonstrates the temperature dependencies of DME conversions over $CuZnAlCe_x$ catalysts. The DME conversion increases with the increase of reaction temperature for all the catalysts. It is observed that at the temperature below 300 °C, there is no distinguishable difference in DME conversion between these catalysts. This is probably limited by the hydrolysis of DME as shown in Eq. (2), because the hydrolysis of DME needs relatively high temperatures on alumina, and it is considered as the rate-determining step for H_2 production via DME SR [9,10]. When the temperature is over 325 °C, noticeable differences in the catalytic performance of different catalysts are observed. It can be seen that the catalysts with 5 or 10 wt% CeO_2 exhibit much better activity for DME conversion as compared with others. At 350 °C, the DME conversion over $CuZnAlCe_{0.1}$ can reach 70.4%, while it is only 55.6% over $CuZnAlCe_0$. However, excess amounts of CeO_2 (>20 wt%) in the catalysts are detrimental to DME SR activity. The enhanced activity of $CuZnAlCe_{0.1}$ could be attributed to its higher copper surface area and better copper dispersion (Table 1). When temperature reaches 425 °C, the nearly full conversion of DME for these two catalysts is achieved. Eguchi et al. [20] ever proposed several assumptions to estimate the apparent activation energy of DME SR over different catalysts, namely: (1) it is a pseudo-first-order reaction, (2) the reactor is an isobaric plug flow reactor, and (3) side reactions are neglected. Based upon these assumptions, corresponding Arrhenius plots for DME SR over $CuZnAlCe_0$ and $CuZnAlCe_{0.1}$ are acquired and displayed in Fig. 8. Rather good linearity is observed, indicating that these assumptions are also acceptable for these two catalysts. By using this method, the apparent activation energies of DME SR over all the catalysts are calculated and listed in Table 1. It is clear that no significant difference exists in the apparent activation energies for these catalysts although their activity differs a lot. This result implies that these catalysts possess similar active sites; the difference in catalytic activity is probably resulted from the different amounts of active sites.

Fig. 9(a) shows the curves of H_2 yield versus reaction temperature over different catalysts. It can be seen that, similar to the DME conversion, the H_2 yield increases with the increase of reaction temperature. Between the temperature region of 400–425 °C, there is a decrease in the H_2 yield. This might be caused

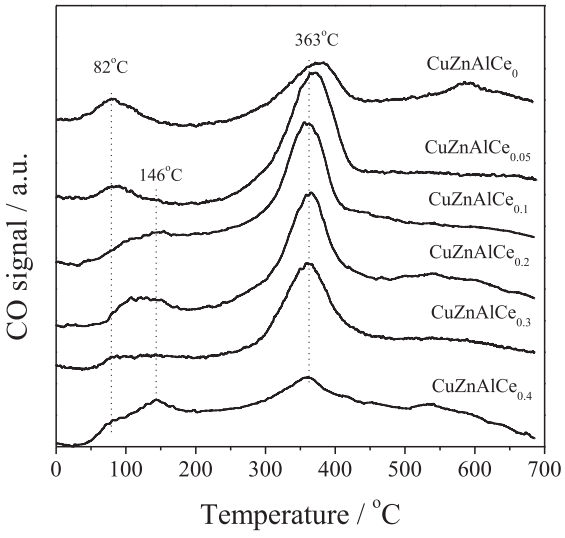

Fig. 6. CO-TPD profiles of the $CuZnAlCe_x$ catalysts pre-reduced by 8% H_2/N_2 (v/v) at 300 °C for 30 min.

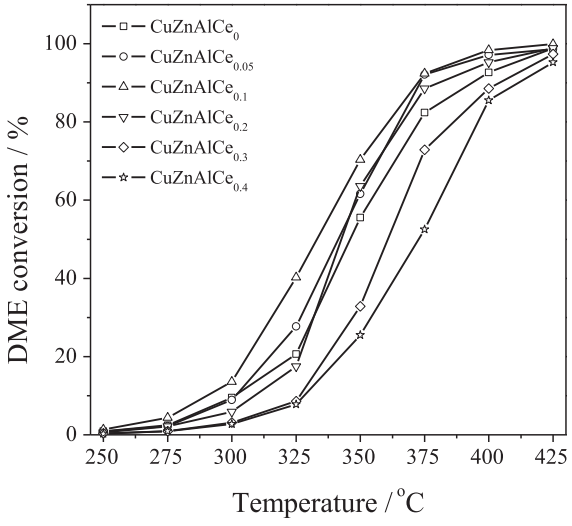

Fig. 7. DME conversion determined at different temperatures over the $CuZnAlCe_x$ catalysts pre-reduced by 10% H_2/N_2 (v/v) at 300 °C for 1 h.

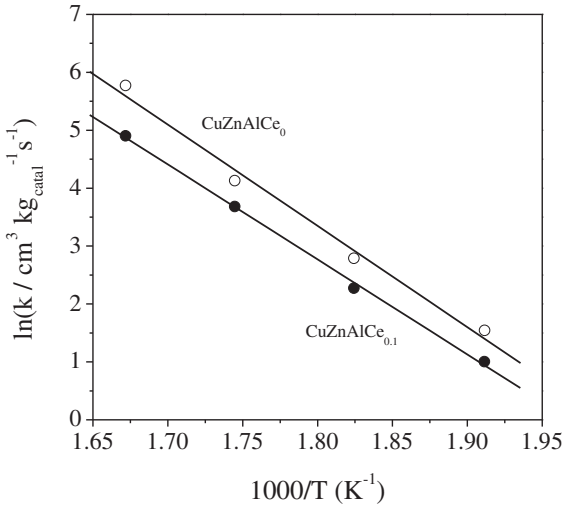

Fig. 8. Arrhenius plots for DME SR over the $CuZnAlCe_0$ and $CuZnAlCe_{0.1}$ catalysts.

by some hydrogen-consumed reactions such as r-WGS reaction shown in Eq. (4). The selectivity to C1 species is also investigated. During DME SR over these catalysts, methanol or other oxygenated compounds were not detected and the selectivity to CH_4 (<1%) was very low and neglected, thus CO_2 and CO are the main carbon-containing products in the reaction temperature range (250–425 °C). Fig. 9(b) and (c) illustrates that CO_2 selectivity decreases and CO selectivity increases with the increase of reaction temperature, which could be caused by several side reactions including the r-WGS reaction in Eq. (4), DME decomposition in Eq. (5), decomposition of MeOH in Eq. (6) and DME to syngas reforming in Eq. (7) at high temperatures [7]. The CO concentration in the reformate gas is considerably lower than the calculated equilibrium value. This is most likely due to the fact that CO_2 is a primary product of DME SR, whereas CO is formed by the reverse water-gas shift reaction which does not reach equilibrium during experiment. By comparison, it is found that the catalyst without Ce shows a little higher CO selectivity, after Ce addition CO selectivity is decreased, which suggests that CO oxidation reaction (WGS) may be enhanced by the presence of Ce due to the improved dispersion of Cu species or CO-chemisorption capability (as shown in

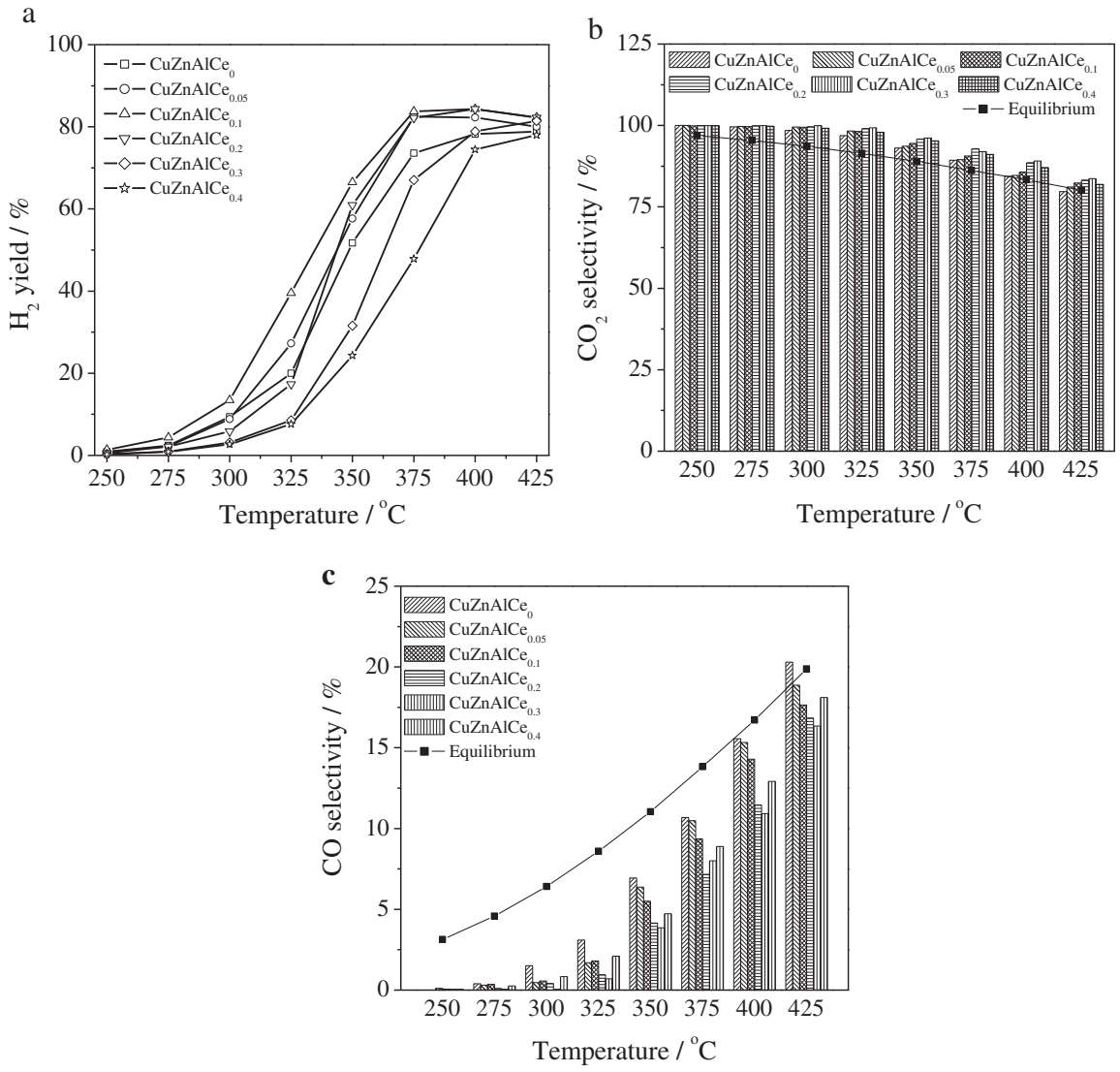

Fig. 9. H_2 yield (a), CO_2 selectivity (b) and CO selectivity (c) determined at different temperatures over $CuZnAlCe_x$ catalysts pre-reduced by 10% H_2/N_2 (v/v) at 300 °C for 1 h.

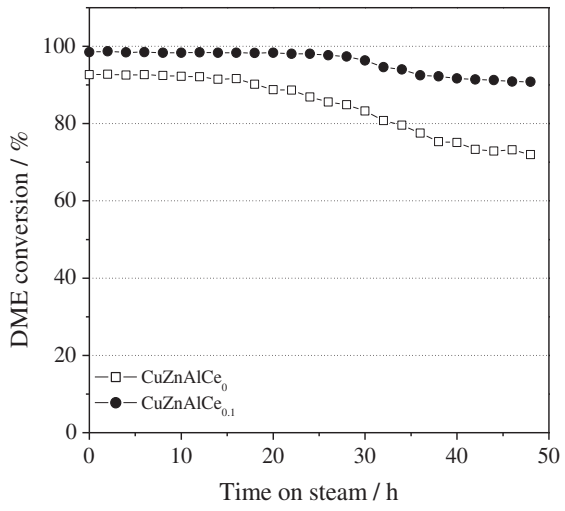

Fig. 10. Time-on-stream stability test for the $CuZnAlCe_0$ and $CuZnAlCe_{0.1}$ catalysts.

the CO-TPD). It should be noted that the CO selectivity exceeds thermodynamic equilibrium value at 425 °C over the $CuZnAlCe_0$ catalyst. The absence of Ce in the catalyst decreases its ability for the oxidation of CO formed via side reactions. The low concentration of CO and high concentration of CO_2 in the products is highly expected for the PEMFCs, so, in this work, the partial substitution of Zn by Ce is particular important.

$$CH_3OCH_{3(g)} \rightarrow CH_{4(g)} + CO_{(g)} + H_{2(g)} \qquad \Delta H^{\ominus} = -1 \text{ kJ mol}^{-1} \quad (5)$$

$$CH_3OH_{(g)} \rightarrow CO_{(g)} + 2H_{2(g)} \qquad \Delta H^{\ominus} = 91 \text{ kJ mol}^{-1} \quad (6)$$

$$CH_3OCH_{3(g)} + H_2O_{(g)} \rightarrow 2CO_{(g)} + 4H_{2(g)} \qquad \Delta H^{\ominus} = 205 \text{ kJ mol}^{-1} \quad (7)$$

3.2.2. Deactivation behavior

It is well known that the main shortcoming of CuZnAl catalysts is their low thermal stability; at the temperature higher than 300 °C the Cu species are readily sintered. To evaluate the thermal stability of the Cu-based catalysts in this work, the two catalysts $CuZnAlCe_0$ and $CuZnAlCe_{0.1}$ are selected and subjected to 48 h durability tests at a relatively higher temperature of 400 °C just for a comparison, the results of which are shown in Fig. 10. It is clear that after 48 h test the DME conversion over $CuZnAlCe_0$ catalyst decreases more than 22%, while it only declines 7.8% over $CuZnAlCe_{0.1}$ catalyst. Obviously, the $CuZnAlCe_{0.1}$ catalyst possesses much higher thermal stability. Fernández-García et al. [26] ever reported that the presence of ceria can improve the thermal stability of Cu-containing catalysts due to the inhibition effect on the sintering of metallic copper phase. In this work, it has been confirmed that the addition of appropriate amounts of CeO_2 to the CuZnAl such as 5 or 10 wt% can obviously increase the dispersion of Cu species. The interaction between ceria and copper species can inhibit the sintering or growth of Cu-related species during DME SR reaction. So, the catalyst $CuZnAlCe_{0.1}$ exhibits much higher thermal stability than $CuZnAlCe_0$.

4. Conclusions

Partially substituted CuZnAlCeO catalysts combined with γ-Al_2O_3 are highly efficient for the production of hydrogen via DME SR route. The optimal substitution amount of CeO_2 in the catalysts is 10 wt%. The presence of appropriate amounts of CeO_2 could not only remarkably increase the performance of the catalysts including DME conversion and H_2 yield, but also greatly improve their thermal stability. Multiple characterization results indicate that the interaction between CeO_2 and Cu species enhances the dispersion of Cu species, effectively inhibiting the sintering of Cu crystallites during DME SR reaction. The Ce-substituted catalysts, especially the two catalysts with 5 and 10 wt% CeO_2, show much stronger capability for CO chemisorption as compared with the one without Ce. XANES fitting results reveal that the presence of ceria can adjust the relative amounts of Cu^0, Cu^+ and Cu^{2+} species. Higher amounts of Cu^+ species exist in the two catalysts containing 5 and 10 wt% CeO_2, which may be related to their better catalytic performance for DME SR to produce H_2.

Acknowledgments

This work is financially supported by the National Natural Science Foundation of China (No. 21076146, 21276184), the Specialized Research Fund for the Doctoral Program of Higher Education of China (No. 20120032110014) and the Program of New Century Excellent Talents in University of China (No. NCET-07-0599). The authors are also grateful to the support from the Program for Introducing Talents of Discipline to Universities of China (No. B06006) and the Engineering Education Funding of Tianjin University.

References

[1] D.E. Curtin, R.D. Lousenberg, T.J. Henry, P.C. Tangeman, M.E. Tisack, J. Power Sources 131 (2004) 41–48.
[2] J. Zhang, Z. Xie, J. Zhang, Y. Tang, C. Song, T. Navessin, Z. Shi, D. Song, H. Wang, D.P. Wilkinson, Z.-S. Liu, S. Holdcroft, J. Power Sources 160 (2006) 872–891.
[3] T.A. Semelsberger, R.L. Borup, J. Power Sources 152 (2005) 87–96.
[4] T.A. Semelsberger, R.L. Borup, H.L. Greene, J. Power Sources 156 (2006) 497–511.
[5] V.A. Sobyanin, S. Cavallaro, S. Freni, Energy Fuels 14 (2000) 1139–1142.
[6] S. Park, B. Choi, B.S. Oh, Int. J. Hydrogen Energy 36 (2011) 6422–6432.
[7] K. Faungnawakij, R. Kikuchi, K. Eguchi, J. Power Sources 164 (2007) 73–79.
[8] K. Faungnawakij, R. Kikuchi, T. Fukunaga, K. Eguchi, Catal. Today 138 (2008) 157–161.
[9] T.A. Semelsberger, K.C. Ott, R.L. Borup, H.L. Greene, Appl. Catal., B 65 (2006) 291–300.
[10] N. Shimoda, K. Faungnawakij, R. Kikuchi, K. Eguchi, Int. J. Hydrogen Energy 36 (2011) 1433–1441.
[11] T.A. Semelsberger, K.C. Ott, R.L. Borup, H.L. Greene, Appl. Catal., B 61 (2005) 281–287.
[12] K. Faungnawakij, R. Kikuchi, T. Matsui, T. Fukunaga, K. Eguchi, Appl. Catal., A 333 (2007) 114–121.
[13] Y. Yamada, T. Mathew, A. Ueda, H. Shioyama, T. Kobayashi, Appl. Surf. Sci. 252 (2006) 2593–2597.
[14] M.D. Rhodes, A.T. Bell, J. Catal. 233 (2005) 198–209.
[15] S. Patel, K.K. Pant, J. Power Sources 159 (2006) 139–143.
[16] P.P.C. Udani, P.V.D.S. Gunawardana, H.C. Lee, D.H. Kim, Int. J. Hydrogen Energy 34 (2009) 7648–7655.
[17] S. Patel, K.K. Pant, Chem. Eng. Sci. 62 (2007) 5436–5443.
[18] R. Kam, C. Selomulya, R. Amal, J. Scott, J. Catal. 273 (2010) 73–81.
[19] P.V. Snytnikov, S.D. Badmaev, G.G. Volkova, D.I. Potemkin, M.M. Zyryanova, V.D. Belyaev, V.A. Sobyanin, Int. J. Hydrogen Energy 37 (2012) 16388–16396.
[20] K. Faungnawakij, T. Fukunaga, R. Kikuchi, K. Eguchi, J. Catal. 256 (2008) 37–44.
[21] X. Wang, X. Pan, R. Lin, S. Kou, W. Zou, J.-X. Ma, Int. J. Hydrogen Energy 35 (2010) 4060–4068.
[22] P. Fornasiero, G. Balducci, R.D. Monte, J. Käspar, V. Sergo, G. Gubitosa, A. Ferrero, M. Graziani, J. Catal. 164 (1996) 173–183.
[23] C.S. Polster, H. Nair, C.D. Baertsch, J. Catal. 266 (2009) 308–319.
[24] J.R. Jensen, T. Johannessen, H. Livbjerg, Appl. Catal., A 266 (2004) 117–122.
[25] J.W. Evans, M.S. Wainwright, A.J. Bridgewater, D.J. Yong, Appl. Catal. 7 (1983) 75–83.
[26] M. Fernández-García, E.G. Rebollo, A.G. Ruiz, J.C. Conesa, J. Soria, J. Catal. 172 (1997) 146–159.
[27] E.B. Fox, S. Velu, M.H. Engelhard, Y.H. Chin, J.T. Miller, J. Kropf, C.S. Song, J. Catal. 260 (2008) 358–370.
[28] A. Martínez-Arias, M. Fernández-García, J. Phys. Chem. C 115 (2011) 23237–23238.
[29] D. Bazin, J.J. Rehr, J. Phys. Chem. C 115 (2011) 23233–23236.

[30] D. Gamarra, M. Fernández-García, C. Belver, A. Martínez-Arias, J. Phys. Chem. C 114 (2010) 18576–18582.
[31] T. Fukunaga, N. Ryumon, S. Shimazu, Appl. Catal., A 348 (2008) 193–200.
[32] D. Gamarra, A. Hornés, Zs. Koppány, Z. Schay, G. Munuera, J. Soria, A. Martínez-Arias, J. Power Sources 169 (2007) 110–116.
[33] T. Caputo, L. Lisi, R. Pirone, G. Russo, Appl. Catal., A 348 (2008) 42–53.
[34] J.P. Breen, J.R.H. Ross, Catal. Today 51 (1999) 521–533.
[35] W.P. Dow, Y.P. Wang, T.J. Huang, Appl. Catal., A 190 (2000) 25–34.
[36] S. Sato, M. Iijima, T. Nakayama, T. Sodesawa, F. Nozaki, J. Catal. 169 (1997) 447–454.
[37] B.A. Peppley, J.C. Amphlett, L.M. Kearns, R.F. Mann, Appl. Catal., A 179 (1999) 31–49.
[38] X. Zhou, M. Meng, Z. Sun, Q. Li, Z. Jiang, Chem. Eng. J. 174 (2011) 400–407.
[39] M.F. Luo, Y.J. Zhong, X.X. Yuan, X.M. Zheng, Appl. Catal., A 162 (1997) 121–131.
[40] F. Bozon-Verduraz, A. Bensalem, J. Chem. Soc. Faraday Trans. 90 (1994) 653–657.